Supporting information

1D:2D Structured AgNW:MXene Composite Transparent Electrode with High Mechanical Robustness for Flexible Photovoltaics

Weipeng Chen[a], Ruijia Zhang[a], Xia Yang[b], Hongyu Wang[a], Hanjun Yang*[b], Xiaotian Hu*[c], Shaohua Zhang*[a]

[a] School of Physics and Materials Science, Nanchang University, 999 Xuefu Avenue, Nanchang 330031, P. R. China

[b] Jiangxi Science & Technology Normal University, Nanchang 330013, Jiangxi, P. R China

[c] School of Chemistry and Chemical Engineering, Institute of Polymers and Energy Chemistry, Nanchang University, Nanchang 330031, P. R. China

*Corresponding author.

E-mail address: yanghj@jxstnu.edu.cn (H. Yang), shz@ncu.edu.cn (S. Zhang), happyhu@ncu.edu.cn (X. Hu)

Author contributions. W. Chen, R. Zhang and X. Yang contributed equally to this work.

Experimental Section

Materials: AgNWs (20 mg/ml in isopropyl alcohol (IPA) with an average diameter of ~ 40 nm and a length of 20-40 μm) were purchased from Nanjing XFNANO Materials Technology Co., Ltd., China. Polyethylene terephthalate (PET) and ITO/PET (the thickness is 125 μm) were purchased from Shenzhen South China Xiangcheng Technology Co., Ltd., China. All the materials and reagents were directly purchased and used without further optimization or purification, including anhydrous N, N-dimethylformamide (DMF, Sigma-Aldrich), anhydrous dimethyl sulfoxide (DMSO, Sigma-Aldrich), anhydrous ethyl alcohol (99.5%, Sigma-Aldrich), lead (II) iodide (PbI_2, 99.999% purity, Afar Aesar), lead bromide ($PbBr_2$, 98%), cesium iodide (CsI, Sigma-Aldrich), methylamine bromine (MABr, >98% purity, Dyesol), methylamine chloride (MACl, >98% purity, Dyesol), formamidinium iodide (FAI, Xi'an p-OLED Corp), bathocuproine (BCP, Sigma-Aldrich), methylamine iodide (MAI) (>98% purity, Dyesol) and [6,6]-phenyl-C_{61}-butyric acid methyl ester ($PC_{61}BM$, American Dye Source Inc), anhydrous isopropanol (IPA,99.5%, Sigma-Aldrich). PEDOT:PSS (Clevios P VP Al4083) was obtained from Heraeus. 1,8-Diiodooctane (DIO) was purchased from Sigma-Aldrich Inc. PM6, BTP-eC9 and PDINO were purchased from Solarmer Materials Inc.

Synthesis and Processing of $Ti_3C_2T_x$ MXene: The $Ti_3C_2T_x$ MXene was synthesized via the chemical liquid phase etching according to the previous literature[1]. To date, the main starting component of MXene is the precursor. $Ti_3C_2T_x$ MXene was made from the transition metal carbide (MAX phase) Ti_3AlC_2 (Ti_3AlC_2 powder was purchased from Jilin 11 technology Co., Ltd.). The morphology of the original Ti_3AlC_2 powder is shown in Figure S1. The common etching methods are minimally intensive layer delamination (MILD) and hydrofluoric acid (HF) etching. Here, we used 30 wt % HF as the etchant. Ti_3AlC_2 powder (0.5 g) was gradually added to 10 ml HF etchant with the help of a magnetic stirrer. The reaction was then carried out for 5 h at a magnetic stirring speed of 400 rpm and a temperature of 35 °C. The reaction mixture was washed with deionized water by centrifugation at 3500 rpm (5 min per cycle) until the pH of the supernatant was about 6 for the first time. Then, the absolute ethanol was added to

the precipitate and sonicated for 1 h (absolute ethanol as intercalation agent), After centrifugal treatment at 10000 rpm for 10 min, the deionized water was added to the centrifuged precipitate, sonicated and centrifuged at 3500 pm, and the upper liquid was delaminated and few layers MXene dispersion. The morphology of multilayered MXene is shown in Figure S1 and the few layers and monolayer MXene are shown in Figure S2. The X-ray diffraction (XRD) patterns of Ti_3AlC_2 powder and $Ti_3C_2T_x$ MXene powder (The powder was obtained by vacuum freeze-drying from the dispersion) are shown in Figure S3. The most intense and representative peak of Ti_3AlC_2 at around 39° that was assigned to (104) disappeared after etching, which indicated the removal of the Al atom in the Ti_3AlC_2. Moreover, the (002) peak broadened and shifted from 9.5° to 5.5°, which implied an increasing interlayer distance. Both the results of scanning electron microscope (SEM) and XRD confirmed the successful synthesis of $Ti_3C_2T_x$ MXene.

Fabrication of AgNW:MXene Transparent Conductive Electrodes: The composite electrodes were fabricated by a spin-coating process. The glass and PET substrates (the whole area is 2.25 cm^2 and the length of a side is 1.5 cm) were ultrasonic cleaned in acetone, deionized water and ethanol for 20 min, respectively and then blown dry by nitrogen (N_2). Then, the substrates were treated with ultraviolet ozone cleaning (UVO) for 20 min to enhance hydrophilicity. AgNWs dispersion was diluted with IPA to a concentration of 5 mg/ml and spin-coated on PET (glass) substrates at a spin-coating speed of 2000 rpm for 60 s. Then, the samples were dried at 50 °C for 5 min. Next, 0.5 mg/ml MXene aqueous suspension was spin-coated on the top of the samples at a spin-coating speed of 2000 rpm for 60 s. Finally, the samples were annealed at 100 °C for 10 min to complete the fabrication of transparent conductive electrodes.

Fabrication of flexible perovskite solar cells: The flexible perovskite solar cells were fabricated on the AgNW:MXene FTEs based on the previous reports[2,3], with the structure of PET/AgNW:MXene/NiO_x/perovskite/$PC_{61}BM$/Ag. NiO_x nanocomposites (NPs) were synthesized by a previously reported method[4]. The NiO_x film as hole transport layer (HTL) was fabricated by meniscus-coating (the blading speed was 10 mm/s and the distance between meniscus and AgNW:MXene FTEs was 50 μm) with a

heating temperature of 55 °C. Then, the NiO_x coated on AgNW:MXene FTEs were annealed at 120 °C for 30 min in air. The perovskite precursor solution was obtained by PbI_2 (742.2 mg), FAI (224.4 mg), MABr (16.2 mg),MACl (20.3 mg), and CsI (19.8 mg) in 1 ml of mixed solvent of DMF/DMSO (volume ratio of 4:1). The composition of the perovskite (PVK) is $Cs_{0.05}FA_{0.85}MA_{0.10}Pb(I_{0.97}Br_{0.03})_3$. The perovskite precursor solution was meniscus-coated on the HTL/AgNW:MXene FTEs (the blading speed was 10 mm/s and the distance between meniscus and HTL/AgNW:MXene FTEs was 100 μm). Next, the HTL/AgNW:MXene FTEs coated with perovskite precursor were annealed on a hot plate at 100 °C for 30 min. Subsequently, the $PC_{61}BM$ (20 mg/ml in anhydrous chlorobenzene) and BCP (0.5 mg/ml in anhydrous ethanol) were deposited by meniscus coating on the perovskite films to form the electron transport layers (ETLs). After drying, Argentum (Ag) metal electrodes (the thickness is 90 nm) were deposited by vacuum evaporation with a high vacuum level of 6×10^{-4} Torr. The preparation process of the test samples was the same as that of the device preparation before evaporation.

Fabrication of flexible organic photovoltaics: The flexible organic photovoltaics were fabricated based on the previous reports[5,6], with the structure of PET/AgNW:MXene/PEDOT:PSS/PM6:BTP-eC9/PDINO/Al. The PEDOT:PSS layer was spin-coated on the AgNW:MXene FTE at 3000 rpm for 30 s and annealed at 150 °C in an ambient atmosphere for 15 min. Then, the PET/AgNW:MXene/PEDOT:PSS substrates were transferred into a glovebox. The polymer donor PM6 solution was prepared in *o*-xylene at 10 mg/ml at 60 °C stirring. BTP-eC9 solution was prepared in *o*-xylene at 10 mg/ml with 0.5% DIO by volume at 80 °C stirring. The PM6 solution was spin-coated on the PET/AgNW:MXene/PEDOT:PSS substrates at 1750 rpm for 60 s to obtain a donor layer. Then, the BTP-eC9 solution was spin-coated on the rotating PM6 donor layer at 2250 rpm for 60 s to obtain an acceptor layer. Afterward, the active layers were thermally annealed at 100 °C for 10 min. Then, PDINO (perylene diimide functionalized with amino N-oxide) was spin-coated on the active layer at 3000 rpm for 30 s. Finally, the device fabrication with the active area of 0.1 cm^2 was completed by thermal evaporation of 100 nm Al as the electrode.

Characterization: The sheet resistance (R_s) of composite transparent conductive electrodes was measured on an ST2263 double testing digital four-probe tester (Suzhou Jingge Electronic Co., Ltd.). The optical transmittance was measured by a UV-vis spectrophotometer (Cary 60, Agilent) from a wavelength range of 350-800 nm. Scanning electron microscope (SEM) images and elemental mapping were taken by using a cold field emission scanning electron microscope (Regulus 8100). The atomic force microscopy (AFM) images and roughness of electrodes were measured by MultiMode 8-HR (Bruker). The transmission electron microscopy (TEM) images were characterized by the transmission electron microscopy (JEOL JEM 2100F) For the ultraviolet photoelectron spectroscopy (UPS) measurements, He I (21.22 eV) radiation line from a discharge lamp was used, with an experimental resolution of 0.15 eV. All the UPS measurements of onset of photoemission for determining the work function were done using standard procedures with a -5 V bias applied to the samples. X-ray diffraction (XRD) was recorded by D8-Discover 25 diffractometer (Bruker). The current density-voltage (*J-V*) was characterized by using Keithley 2400 Sourcemeter. The currents were measured under the solar simulator (Enli Tech, 100 mW/cm^2, AM 1.5 G irradiation) and the reference silicon solar cell was corrected from NREL. All the measurements were performed under nitrogen at room temperature. The scan range was from 0 V to 1.2 V, with 8.0 mV for each step. The scan rate was 0.2 V/s and the delay time was 30 ms. The EQE spectra were recorded on a commercial EQE measurement system (Enlitech, QE-R3011).

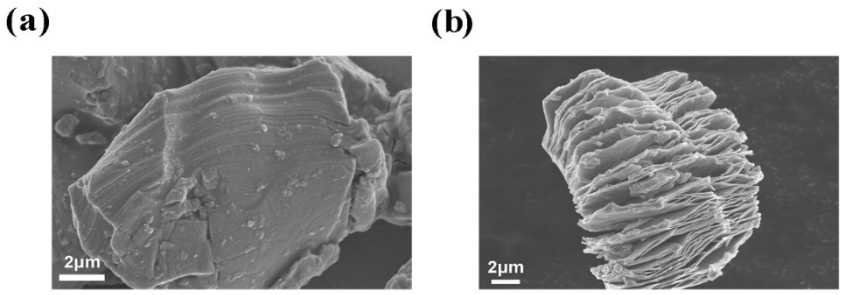

Figure S1. SEM images of (a) Ti_3AlC_2 MAX, (b) multilayered $Ti_3C_2T_x$ MXene after etching with HF.

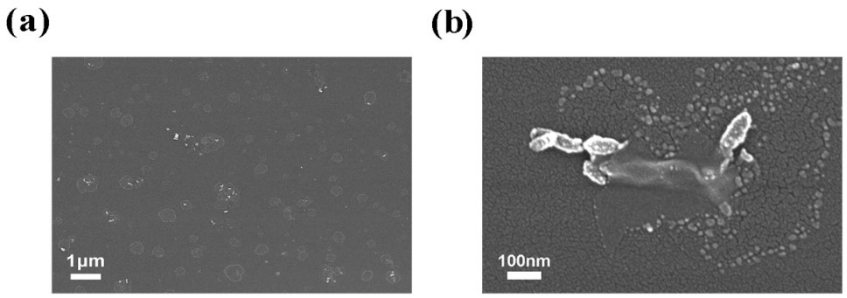

Figure S2. SEM images of (a) few layers and monolayer $Ti_3C_2T_x$ MXene after centrifugal intercalation separation and (b) the monolayer of $Ti_3C_2T_x$ MXene.

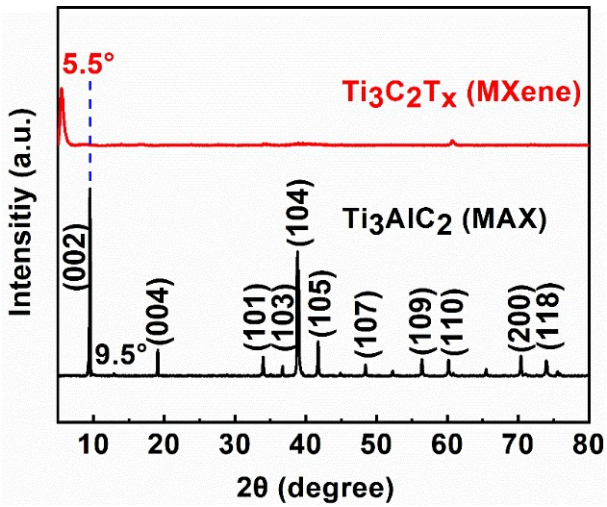

Figure S3. XRD patterns of Ti_3AlC_2 (MAX) and delaminated $Ti_3C_2T_x$ (MXene) after HF etching.

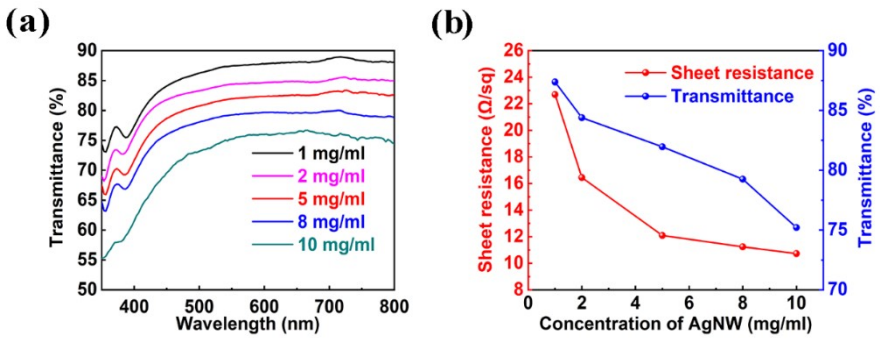

Figure S4. (a) Transmittance spectra and (b) R_s and transmittance (550 nm) of AgNW electrodes prepared from AgNW dispersion with various concentrations.

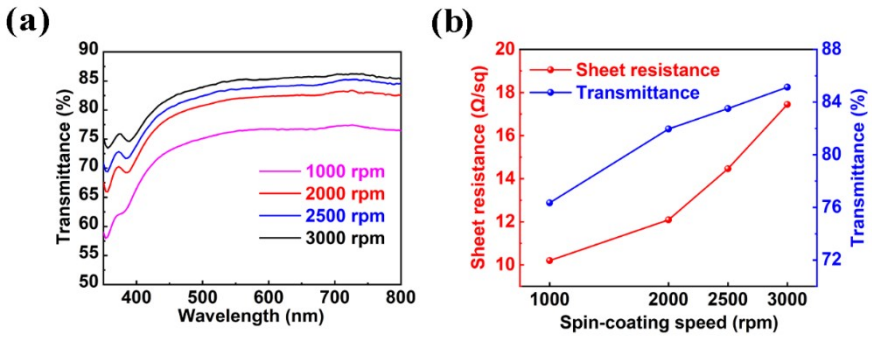

Figure S5. (a) Transmittance spectra and (b) R_s and transmittance (550 nm) of AgNW electrodes prepared from 5 mg/ml AgNW dispersion with different spin-coating speeds.

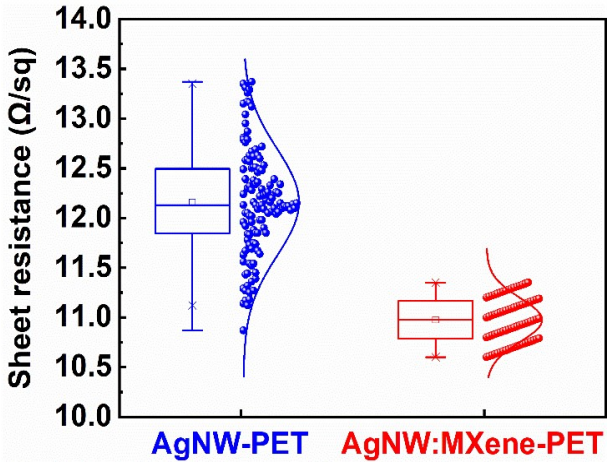

Figure S6. Box plot and normal distribution curve of R_s from AgNW-PET and AgNW:MXene-PET electrodes.

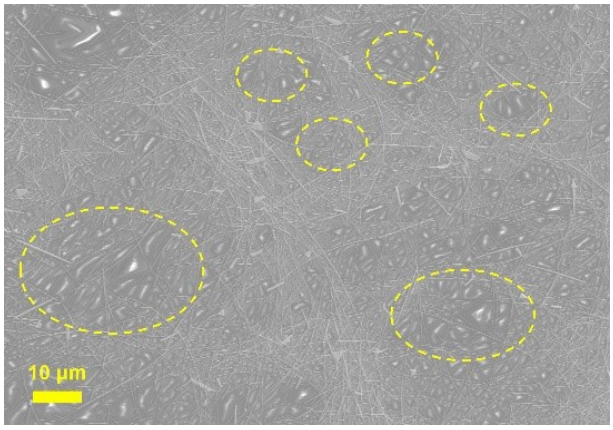

Figure S7. SEM image of pristine AgNW network (the voids that generated by the random arrangement of AgNWs).

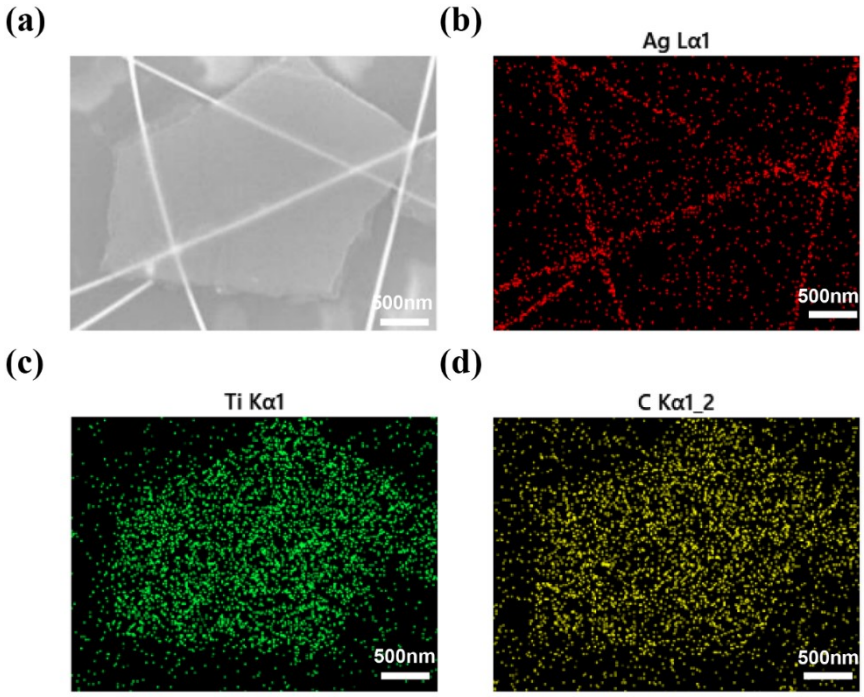

Figure S8. SEM images of the 1D:2D AgNW:MXene composite welding structure and the surface elemental analysis of silver (Ag), titanium (Ti) and carbon (C) elements.

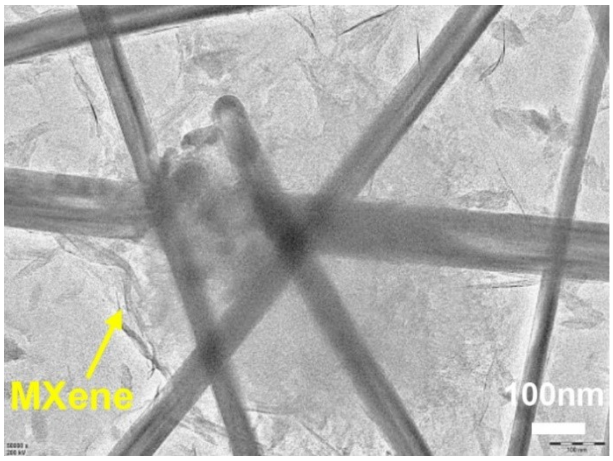

Figure S9. TEM image of the welding structure of AgNW:MXene FTE.

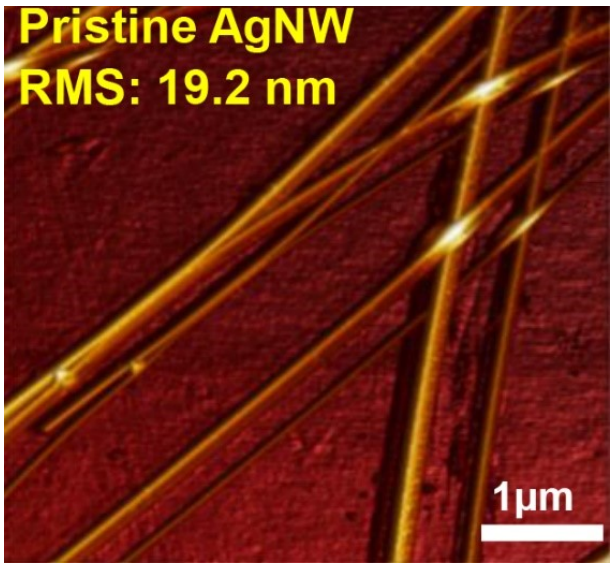

Figure S10. AFM image of the pristine AgNW FTE.

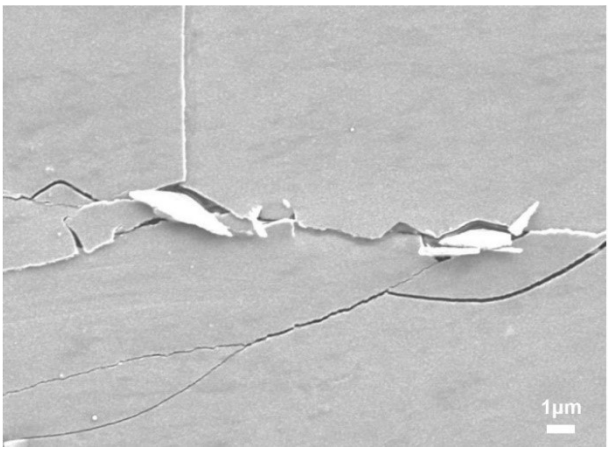

Figure S11. SEM image of ITO-PET after the mechanical bending tests with bending 1000 times at a curvature of 5 mm.

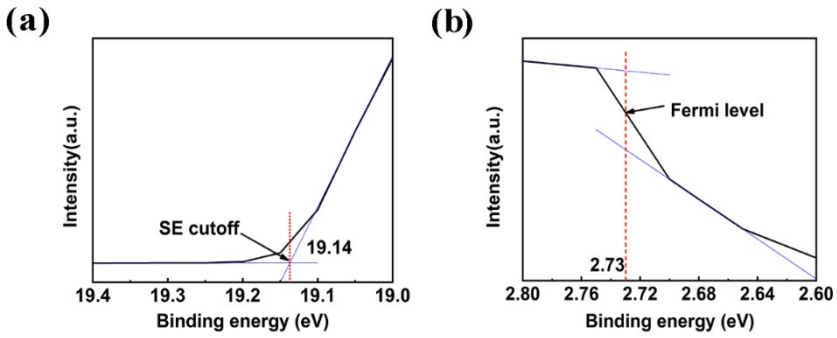

Figure S12. UPS spectra of AgNW:MXene film. The photon energy of excitation source He I is 21.2 eV. (a) Secondary electron cutoff edge spectrum. The SE cutoff is 19.14 eV. (b) Fermi edge spectrum. The Fermi level is 2.73 eV. The work function is 4.81 eV.

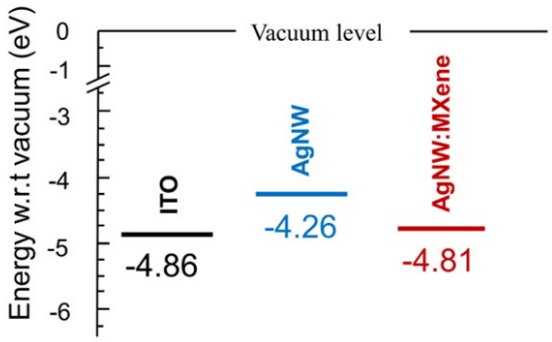

Figure S13. The work function of ITO-PET, AgNW-PET and AgNW:MXene-PET.

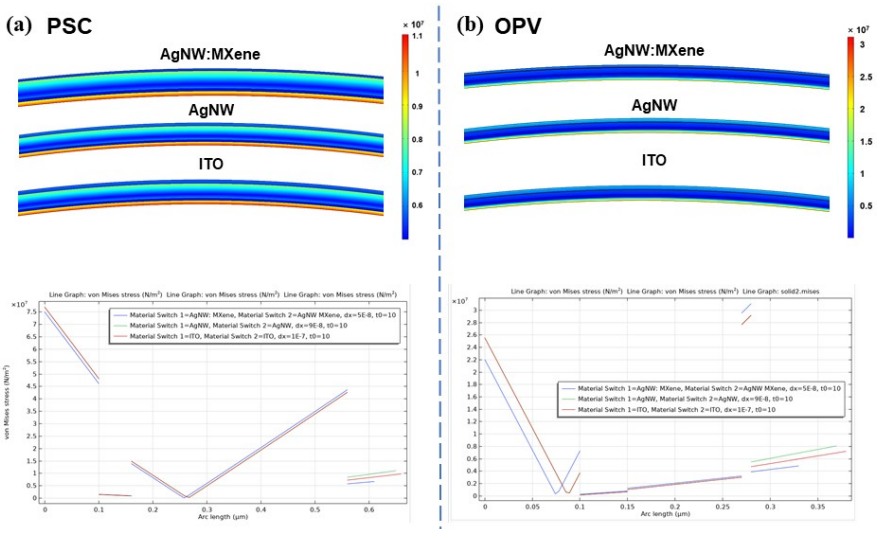

Figure S14. Finite-element simulation of PSCs and OPVs with ITO, AgNW, and AgNW:MXene electrodes.

The finite-element simulation with the structure of the flexible PSC and OPV with ITO, AgNW, and AgNW:MXene electrodes were constructed. By using the Young's Modulus, Poisson ratio, and film thickness for each layer, the stress distribution of the whole devices in the bending process is simulated.

Table S1. Photoelectric performance of AgNW electrodes fabricated by different concentrations of AgNW dispersion.

Concentration of AgNW (mg/ml)	T_{550nm} (%)[a),b)]	R_s (Ω/sq) [a)]	FoM
1	87.38	22.69±3.52	119.06
2	84.39	16.45±2.36	129.38
5	81.96	12.09±2.04	149.08
8	79.25	11.24±1.88	136.00
10	75.21	10.73±1.65	114.76

[a)] The average values of sheet resistance and transmittance were calculated from more than 10 electrodes. [b)] Note that the transmittance shown here does not include the substrate (i.e. using the substrate as reference).

Table S2. Photoelectric performance of AgNW electrodes fabricated by 5 mg/ml AgNW dispersion at different spin-coating speeds.

Spin-coating speed (rpm)	T_{550nm} (%)[a),b)]	R_s (Ω/sq) [a)]	FoM
1000	76.35	10.20±1.47	127.94
2000	81.96	12.09±1.96	149.08
2500	83.51	14.46±2.61	138.26
3000	85.13	17.45±3.28	128.87

[a)] The average values of sheet resistance and transmittance were calculated from more than 10 electrodes. [b)] Note that the transmittance shown here does not include the substrate (i.e. using the substrate as reference).

Table S3. The transmittance (at the wavelength of 550 nm), sheet resistance and FoM of different electrodes that reported in other references. (CNT: carbon nanotube, GO: graphene oxide, AZO: aluminum-doped zinc oxide, PEDOT:PSS: poly(3,4-ethylenedioxythiophene): poly(styrene sulfonic acid), PI: polyimide)

Electrode type	T_{550nm} (%)	R_s (Ω/sq)	FoM
This work	82.84	10.91	175.05
AgNW/CNT[7]	94.5	50	131.41
AgNW/GO[8]	80	27	59.15
AgNW (spray-coating)[9]	86	30	80.22
AgNW (spin-coating)[10]	94	50.3	119.27
Printed AgNW[11]	80	10	159.7
AgNW/AZO[12]	88.2	23.1	125.94
PEDOT:PSS[13]	90	45	77.44
AgNW:ZnO[14]	80	28	57.04
AgNW:PI[15]	83.2	26	75.27
Graphene[16]	93	40	127.53

Table S4. Mechanical properties of flexible electrodes and flexible PSCs for finite-element simulation.

Materials	Thickness (μm)	Young's modulus (GPa)	Density (ρ, g cm^{-3})	Poisson's ratio
ITO	0.1	0.96	6.80	0.35
AgNW	0.09	1.15	5.0	0.29
AgNW:MXene	0.05	0.78	5.5	0.15
PVK	0.4	5.90	4.1	0.23
PCBM	0.06	0.38	1.6	0.36
Ag	0.1	11.4	10.5	0.38

Table S5. Mechanical properties of flexible electrodes and flexible OPVs for finite-element simulation.

Materials	Thickness (μm)	Young's modulus (GPa)	Density (ρ, g cm^{-3})	Poisson's ratio
ITO	0.1	0.96	6.80	0.35
AgNW	0.09	1.15	5.0	0.29
AgNW:MXene	0.05	0.78	5.5	0.15
PEDOT:PSS	0.01	5.90	1.41	0.36
Active Layer	0.12	0.678	1.75	0.21
PDINO	0.05	0.427	0.8	0.30
Al	0.1	68.2	2.7	0.30

The Young's Modulus is measured by the peak-force model of AFM. Young's Modulus is a common parameter in engineering design for selecting the materials of mechanical parts and is also a physical quantity describing the deformation resistance of solid materials.

References

1. M. Alhabeb, K. Maleski, B. Anasori, P. Lelyukh, L. Clark, S. Sin and Y. Gogotsi, Chem. Mater. 29 (2017) 7633-7644.
2. X. Meng, Z. Cai, Y. Zhang, X. Hu, Z. Xing, Z. Huang, Z. Huang, Y. Cui, T. Hu, M. Su, X. Liao, L. Zhang, F. Wang, Y. Song and Y. Chen, Nat Commun. 11 (2020) 3016.
3. X. Meng, Z. Xing, X. Hu, Z. Huang, T. Hu, L. Tan, F. Li and Y. Chen, Angew. Chem. Int. Ed. Engl. 59 (2020) 16602-16608.
4. H. Wang, Z. Huang, S. Xiao, X. Meng, Z. Xing, L. Rao, C. Gong, R. Wu, T. Hu, L. Tan, X. Hu, S. Zhang and Y. Chen, J. Mater. Chem. A. 9 (2021) 5759-5768.
5. S. Liu, D. Chen, X. Hu, Z. Xing, J. Wan, L. Zhang, L. Tan, W. Zhou and Y. Chen, Adv. Funct. Mater. 30 (2020) 2003223.
6. Y. Zhang, K. Liu, J. Huang, X. Xia, J. Cao, G. Zhao, P. W. K. Fong, Y. Zhu, F. Yan, Y. Yang, X. Lu and G. Li, Nat Commun. 12 (2021) 4815.
7. D. Kim, L. Zhu, D-J. Jeong, K. Chun, Y-Y. Bang, S-R. Kim, J-H. Kim and S-K. Oh, Carbon. 63 (2013) 530-536.
8. X. Zhang, X. Yan, J. Chen and J. Zhao, Carbon. 69 (2014) 437-443.
9. Z. Yu, L. Li, Q. Zhang, W. Hu and Q. Pei, Adv. Mater. 23 (2011) 4453-4457.
10. Y. Jin, L. Li, Y. Cheng, L. Kong, Q. Pei and F. Xiao, Adv. Funct. Mater. 25 (2015) 1581-1587.
11. F. Guo, N. Li, V. V. Radmilović, V. R. Radmilović, M. Turbiez, E. Spiecker, K. Forberich and C. J. Brabec, Energy Environ. Sci. 8 (2015) 1690-1697.
12. T. Y. Qu, L. J. Zuo, J. D. Chen, X. Shi, T. Zhang, L. Li, K. C. Shen, H. Ren, S. Wang and F. M. Xie, Adv. Opt. Mater. 8 (2020) 2000669.
13. N. Kim, H. Kang, J. H. Lee, S. Kee, S. H. Lee and K. Lee, Adv. Mater. 27 (2015) 2317-2323.
14. Y.-X. Zhang, J. Fang, W. Li, Y. Shen, J.-D. Chen, Y. Li, H. Gu, S. Pelivani, M. Zhang and Y. Li, ACS Nano, 13 (2019) 4686-4694.
15. X. Dong, P. Shi, L. Sun, J. Li, F. Qin, S. Xiong, T. Liu, X. Jiang and Y. Zhou, J. Mater. Chem. A. 7 (2019) 1989-1995.

16. B. Deng, P.-C. Hsu, G. Chen, B. Chandrashekar, L. Liao, Z. Ayitimuda, J. Wu, Y. Guo, L. Lin and Y. Zhou, Nano Lett. 15 (2015) 4206-4213.